

Cardiac electrical defects in progeroid mice and Hutchinson–Gilford progeria syndrome patients with nuclear lamina alterations

José Rivera-Torres^{a,1}, Conrado J. Calvo^{a,b,c,2}, Anna Llach^{d,2}, Gabriela Guzmán-Martínez^{a,e,2}, Ricardo Caballero^f, Cristina González-Gómez^a, Luis J. Jiménez-Borreguero^{a,g}, Juan A. Guadix^{h,i}, Fernando G. Osorio^j, Carlos López-Otín^j, Adela Herraiz-Martínez^{d,k}, Nuria Cabello^{d,k}, Alex Vallmitjana^l, Raul Benítez^l, Leslie B. Gordon^{m,n,o}, José Jalife^{a,p,q}, José M. Pérez-Pomares^{h,i}, Juan Tamargo^f, Eva Delpón^f, Leif Hove-Madsen^{d,k}, David Filgueiras-Rama^{a,r}, and Vicente Andrés^{a,3}

^aCentro Nacional de Investigaciones Cardiovasculares Carlos III (CNIC), 28029 Madrid, Spain; ^bGroup Electrophysiology and Bioengineering (GEB), Information and Communication Technologies Institute (ITACA), Universitat Politècnica de València, 46022 Valencia, Spain; ^cDepartment of Physiology, Facultad de Medicina y Odontología, Universidad de Valencia, 46010 Valencia, Spain; ^dInstitut d'Investigació Biomedica Sant Pau, Hospital de Sant Pau, 08025 Barcelona, Spain; ^eCardiac Imaging Unit, Cardiology Department, Hospital Universitario La Paz, IdiPaz, 28046 Madrid, Spain; ^fDepartment of Pharmacology, School of Medicine, Universidad Complutense, 28040 Madrid, Spain; ^gServicio de Cardiología, Hospital de la Princesa, 28006 Madrid, Spain; ^hDepartment of Animal Biology, Instituto de Investigación Biomédica de Málaga (IBIMA), University of Málaga, 29071 Málaga, Spain; ⁱCentro Andaluz de Nanomedicina y Biotecnología (BIONAND), Junta de Andalucía, Universidad de Málaga, 29590 Campanillas, Spain; ^jDepartamento de Bioquímica y Biología Molecular, Instituto Universitario de Oncología, Universidad de Oviedo, 33006 Oviedo, Spain; ^kCardiovascular Research Center, Hospital de Sant Pau, 08025 Barcelona, Spain; ^lAutomatic Control Department, Universitat Politècnica de Catalunya, 08034 Barcelona, Spain; ^mDepartment of Pediatrics, Alpert Medical School of Brown University, Providence, RI 02903; ⁿDepartment of Pediatrics, Hasbro Children's Hospital, Providence, RI 02903; ^oDepartment of Anesthesia, Division of Critical Care Medicine, Boston Children's Hospital and Harvard Medical School, Boston, MA 02115; ^pDepartment of Internal Medicine, University of Michigan, Ann Arbor, MI 48109; ^qCenter for Arrhythmia Research, University of Michigan, Ann Arbor, MI 48109-2800; and ^rDepartment of Cardiology, Cardiac Electrophysiology Unit, Hospital Clínico San Carlos, 28040 Madrid, Spain

Edited by J. G. Seidman, Harvard Medical School, Boston, MA, and approved October 3, 2016 (received for review March 8, 2016)

Hutchinson–Gilford progeria syndrome (HGPS) is a rare genetic disease caused by defective prelamin A processing, leading to nuclear lamina alterations, severe cardiovascular pathology, and premature death. Prelamin A alterations also occur in physiological aging. It remains unknown how defective prelamin A processing affects the cardiac rhythm. We show age-dependent cardiac repolarization abnormalities in HGPS patients that are also present in the *Zmpste24*^{-/-} mouse model of HGPS. Challenge of *Zmpste24*^{-/-} mice with the β-adrenergic agonist isoproterenol did not trigger ventricular arrhythmia but caused bradycardia-related premature ventricular complexes and slow-rate polymorphic ventricular rhythms during recovery. Patch-clamping in *Zmpste24*^{-/-} cardiomyocytes revealed prolonged calcium-transient duration and reduced sarcoplasmic reticulum calcium loading and release, consistent with the absence of isoproterenol-induced ventricular arrhythmia. *Zmpste24*^{-/-} progeroid mice also developed severe fibrosis-unrelated bradycardia and PQ interval and QRS complex prolongation. These conduction defects were accompanied by overt mislocalization of the gap junction protein connexin43 (Cx43). Remarkably, Cx43 mislocalization was also evident in autopsied left ventricle tissue from HGPS patients, suggesting intercellular connectivity alterations at late stages of the disease. The similarities between HGPS patients and progeroid mice reported here strongly suggest that defective cardiac repolarization and cardiomyocyte connectivity are important abnormalities in the HGPS pathogenesis that increase the risk of arrhythmia and premature death.

Hutchinson–Gilford progeria syndrome | progerin | prelamin A | connexin43 | calcium handling

The *LMNA* gene encodes A-type lamins (lamin A and lamin C), key components of the mammalian nuclear envelope with important structural and regulatory functions that affect signaling, transcription, and chromatin organization among other processes (1). Mature lamin A is produced from the precursor prelamin A through a series of posttranslational modifications, consisting of sequential farnesylation at the cysteine in the Cysteine-Serine-Isoleucine-Methionine motif, cleavage of the Serine-Isoleucine-Methionine residues, carboxymethylation of the newly accessible cysteine, and a final proteolytic cleavage by the zinc metallopeptidase STE24 (ZMPSTE24, also called FACE-1) (2).

Mutations in the human *LMNA* gene or defective processing of prelamin A cause a group of diseases termed laminopathies, including the premature aging disorder Hutchinson–Gilford progeria syndrome (HGPS), a very rare genetic disorder with an estimated prevalence of 1 in 21 million people (www.progeriaresearch.org).

Significance

Defective prelamin A processing causes cardiovascular alterations and premature death in Hutchinson–Gilford progeria syndrome (HGPS) patients and also occurs during physiological aging. We found overt repolarization abnormalities in HGPS patients at advanced disease stages. Similar alterations were present in progeroid *Zmpste24*^{-/-} mice, which had cardiomyocytes that exhibited prolonged calcium transient duration and reduced sarcoplasmic reticulum calcium loading capacity and release, consistent with absence of isoproterenol-induced ventricular arrhythmias. *Zmpste24*^{-/-} mice developed age-dependent bradycardia and PQ interval/QRS complex prolongation, likely contributing to premature death. These defects correlated with mislocalization of connexin43, which was also noted in heart tissue from HGPS patients. These results reveal molecular alterations that might cause cardiac rhythm alterations and premature death in HGPS.

Author contributions: J.R.-T., R.C., J.J., J.T., E.D., L.H.-M., D.F.-R., and V.A. designed research; J.R.-T., C.J.C., G.G.-M., R.C., C.G.-G., L.J.J.-B., J.A.G., A.H.-M., N.C., A.V., R.B., J.M.P.-P., J.T., and L.H.-M. performed research; J.R.-T., C.J.C., A.L., G.G.-M., R.C., L.J.J.-B., F.G.O., L.B.G., J.M.P.-P., J.T., E.D., L.H.-M., D.F.-R., and V.A. analyzed data; C.G.-G. generated and maintained mice and cells; F.G.O. and C.L.O. generated and maintained mice; V.A. coordinated the study; and J.R.-T., C.J.C., C.L.O., L.B.G., J.J., J.M.P.-P., E.D., L.H.-M., D.F.-R., and V.A. wrote the paper.

The authors declare no conflict of interest.

This article is a PNAS Direct Submission.

Freely available online through the PNAS open access option.

¹Present address: Faculty of Biomedical Science, European University of Madrid, 28670 Villaviciosa de Odón, Madrid, Spain.

²C.J.C., A.L., and G.G.-M. contributed equally to this work.

³To whom correspondence should be addressed. Email: vandres@cnic.es.

This article contains supporting information online at www.pnas.org/lookup/suppl/doi:10.1073/pnas.1603754113/DCSupplemental.

HGPS patients exhibit accelerated atherosclerosis and arterial stiffness, leading to premature death at an average age of 14.6 y, predominantly from myocardial infarction, heart failure, or stroke (3, 4). Most HGPS patients carry a noninherited de novo heterozygous synonymous mutation in the *LMNA* gene (c.1824C > T: GGC > GGT; p.G608G), which activates the use of an internal 5' splicing site in exon 11 that causes the synthesis of progerin. This unprocessed form of prelamin A lacks 50 amino acids encompassing the ZMPSTE24 cleavage site and therefore, remains permanently farnesylated (2). *ZMPSTE24* mutations have also been linked to several other human progeroid syndromes (5, 6), reinforcing the notion that accumulation of progerin or prelamin A accelerates cellular aging. Moreover, progerin and prelamin A are both expressed in cells and tissues of normally aging non-HGPS individuals, suggesting their involvement in physiological aging (reviewed in refs. 2 and 7).

Genetically modified mice expressing prelamin A or progerin have enabled the study of mechanisms underlying progeria (8) and testing of the efficacy of various therapies (9, 10). Here, we examined cardiac electrical alterations in 15 HGPS patients with the classical *LMNA* c.1824C > T mutation, representing ~5% of

the world population (www.progeriaresearch.org). We then correlated the observed alterations in HGPS patients to the underlying molecular processes in *Zmpste24*-null mice; these mice accumulate farnesylated prelamin A in the nuclear envelope and phenocopy several other defects observed in HGPS, including cardiovascular alterations and premature death (average lifespan ~20 wk vs. >2 y in WT mice) (9, 11).

Results

Electrocardiographic Alterations in HGPS Patients. *SI Appendix, Tables S1 and S2* show electrocardiographic measurements from HGPS patient carriers of the *LMNA* c.1824C > T mutation ($n = 15$, age range 2–19 y old) and controls ($n = 13$, age range 4–19 y old), respectively. A glossary of electrocardiographic parameters can be found in *SI Appendix*. As they aged, seven patients showed overt repolarization abnormalities in at least one electrocardiogram (ECG) that were compatible with coronary artery disease (ST segment depression/elevation and negative and biphasic T waves) (a representative example is in *SI Appendix, Fig. S1A*). One patient showed significant QTc interval prolongation (537 ms) in the context of ischemia at advanced stages of the

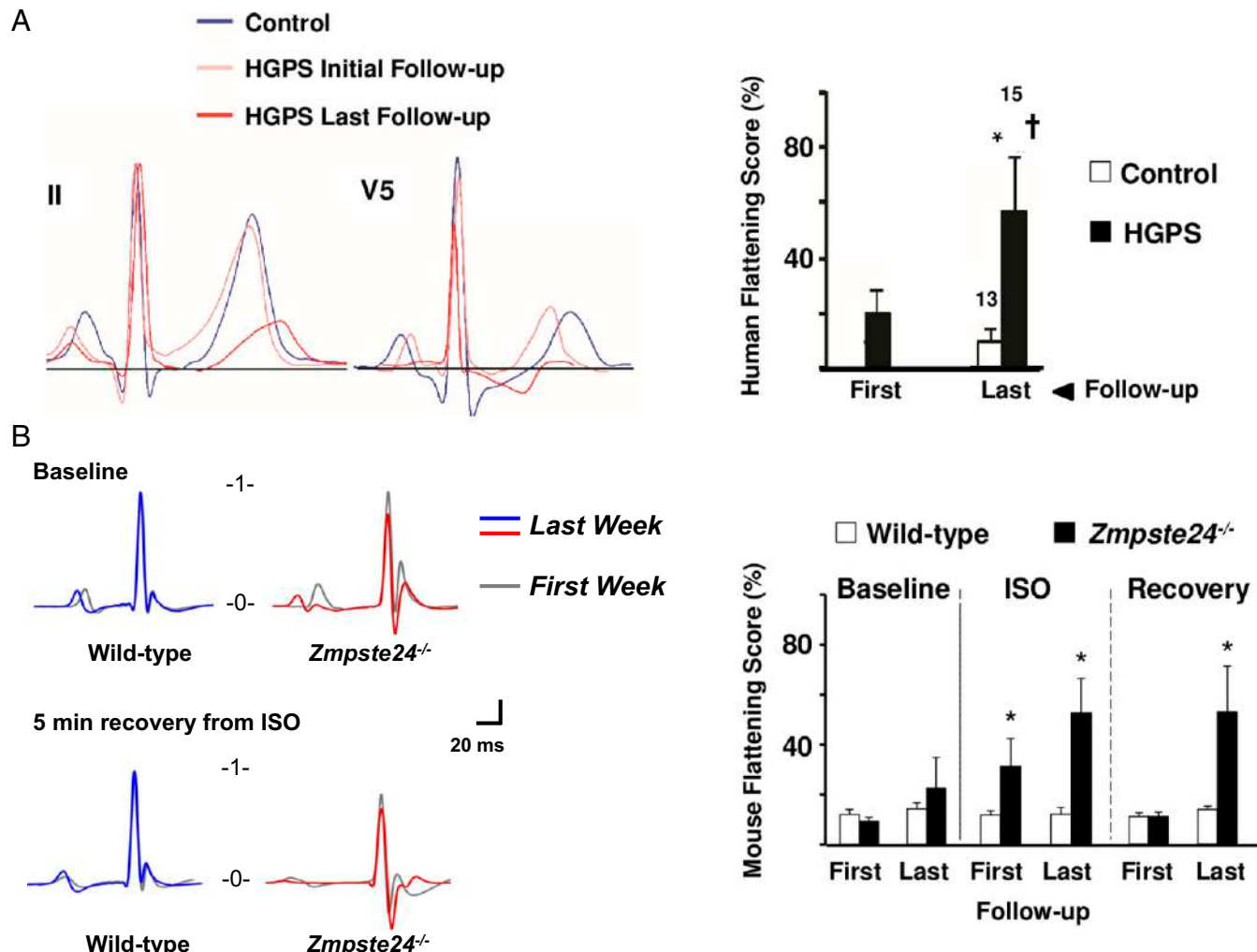


Fig. 1. Age-related exacerbation of repolarization abnormalities in HGPS patients and *Zmpste24*^{-/-} mice. (A, Left) Extracted averaged ECG leads II and V5 from human control participants (blue traces) and HGPS patients at initial stage (Initial; light red trace) and advanced stages (Last; dark red trace). (A, Right) Quantification of mean flattening scores. (B, Left) Representative T-wave abnormalities in *Zmpste24*^{-/-} mice comparing the first and the last isoproterenol (ISO) challenge (*SI Appendix, SI Materials and Methods*). (B, Right) Mean effective flattening scores at baseline, after ISO exposure and during 5-min recovery. *P < 0.05 vs. control; †P < 0.05 vs. first follow-up. First: 11-wk-old mice; Last: 19-wk-old mice or last week before death.

disease (18 y of age). These alterations were not observed in controls (a representative example is in *SI Appendix*, Fig. S1B). Repolarization abnormalities in HGPS patients were highly evident at advanced disease stages. Compared with age-matched controls, HGPS patients exhibited significant T-wave flattening, which was exacerbated as disease progressed (Fig. 1A, initial: initial ECG; last: last ECG during follow-up). All patients and controls had sinus rhythm and normal PR interval and QRS complex duration (*SI Appendix*, Tables S1 and S2). Interestingly, although all HGPS patients exhibited cardiac rhythm within physiological values, the heart rate and PR interval tended to be slower and larger, respectively, in older HGPS patients (6 of 15) at the end of the follow-up period (26.8 ± 2.3 mo follow-up): heart rates on first and last ECGs were 114 ± 7 and 101 ± 7 beats per minute (bpm), respectively, $P = 0.36$; PRs on first and last ECGs were 115 ± 2 and 128 ± 11 ms, respectively, $P = 0.22$.

Time Course of ECG Abnormalities in Progeroid *Zmpste24*^{-/-} Mice. We next analyzed the electrocardiographic phenotype of *Zmpste24*^{-/-} mice, an established preclinical model of HGPS (9, 11). A glossary of electrocardiographic parameters can be found in *SI Appendix*. To study repolarization, we quantified T-wave flattening by measuring T-wave morphology changes, including

sharpness, by excess kurtosis of the T-wave peak in relation to its geometrical change from the isoelectric line and the area under the T wave (*SI Appendix*, *SI Materials and Methods*). Similar to HGPS patients, progeroid mice showed repolarization abnormalities manifested as significant T-wave flattening. To determine the risk of ventricular arrhythmia associated with T-wave alterations, we used the β -adrenergic agonist isoproterenol, which can trigger calcium-related alterations in cardiac repolarization. Weekly isoproterenol challenge, based on its sympathomimetic effect and ability to induce Ca^{2+} -related alterations in repolarization, further exacerbated the repolarization alterations as *Zmpste24*^{-/-} mice aged, although acute isoproterenol did not cause significant ventricular arrhythmias in *Zmpste24*^{-/-} or controls (Fig. 1B). Although both groups responded normally in the first week of follow-up, older *Zmpste24*^{-/-} mice developed a very marked reduction in the heart rate (bradycardia) during recovery from isoproterenol (Fig. 2A). In addition, compared with WT controls, *Zmpste24*^{-/-} mice progressively developed longer RR intervals as they aged (Fig. 2B and C). The variability of the RR interval, measured as the SD, increased linearly as a function of the average RR interval (*SI Appendix*, Fig. S2) and was associated with increased incidence of premature ventricular complexes (Fig. 2D and *SI Appendix*, Fig. S3) and a short lifespan.

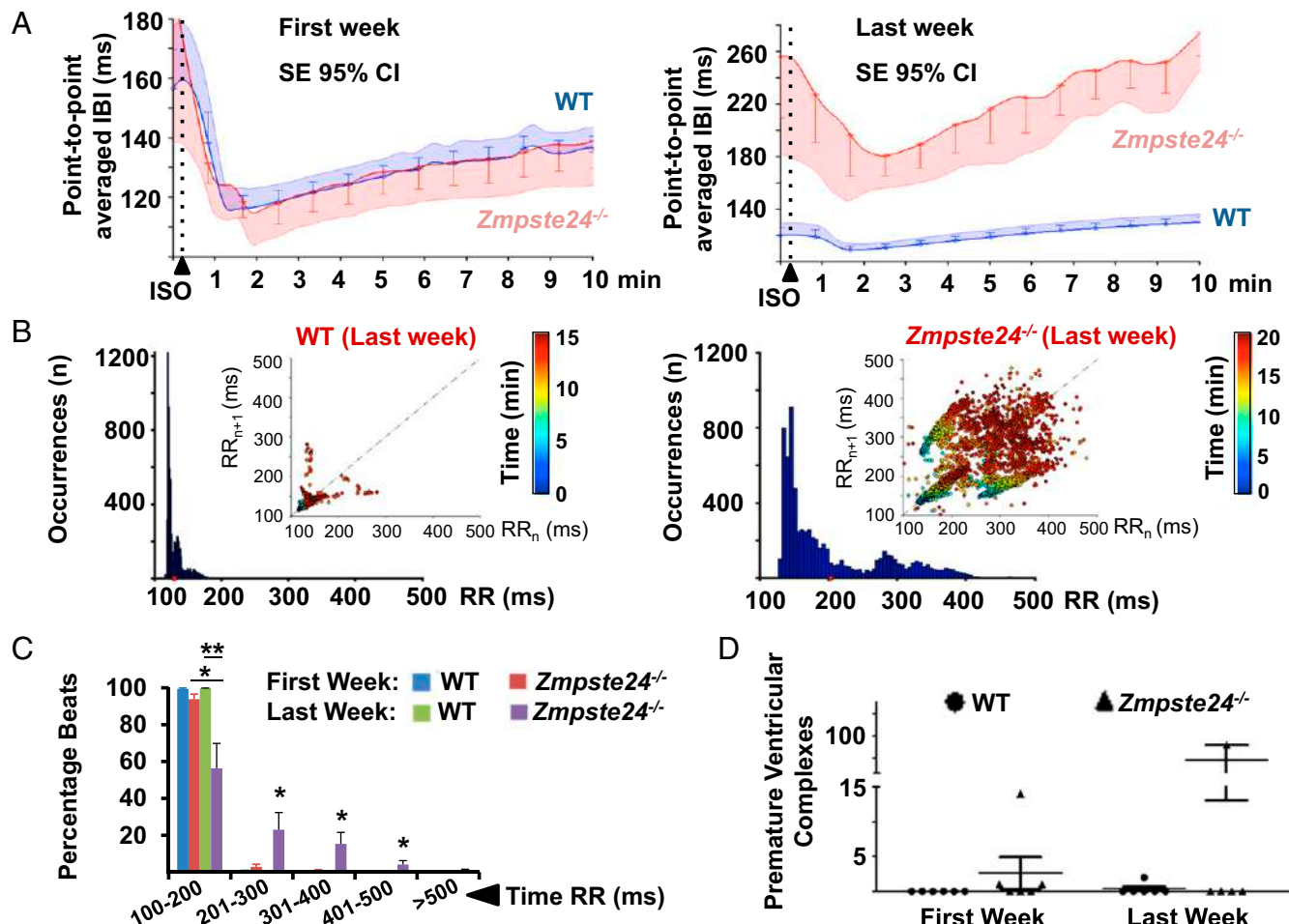


Fig. 2. Severe bradycardia in postisoproterenol (post-ISO) administration recovery is associated with an increase in premature ventricular complexes in *Zmpste24*^{-/-} mice. First: 11-wk-old mice; Last: 19-wk-old mice or last week before death. (A) β -Adrenergic response [interbeat interval (IBI)] in WT and *Zmpste24*^{-/-} mice from the first to the last ISO challenge. 95% CI, 95% confidence interval. (B) RR histograms in WT and *Zmpste24*^{-/-} mice during ISO time course challenge. The insets show correlation plots between consecutive cardiac beats (RR_n vs. RR_{n+1}; n = cardiac beat number within the entire registration period; color-coded timescale). A significant increase in the percentage of long RR intervals during the last week of follow-up (C) was also associated with a significant increase in bradycardia-related premature ventricular complexes (D). * $P < 0.05$; ** $P < 0.01$ (*SI Appendix*, *SI Materials and Methods*).

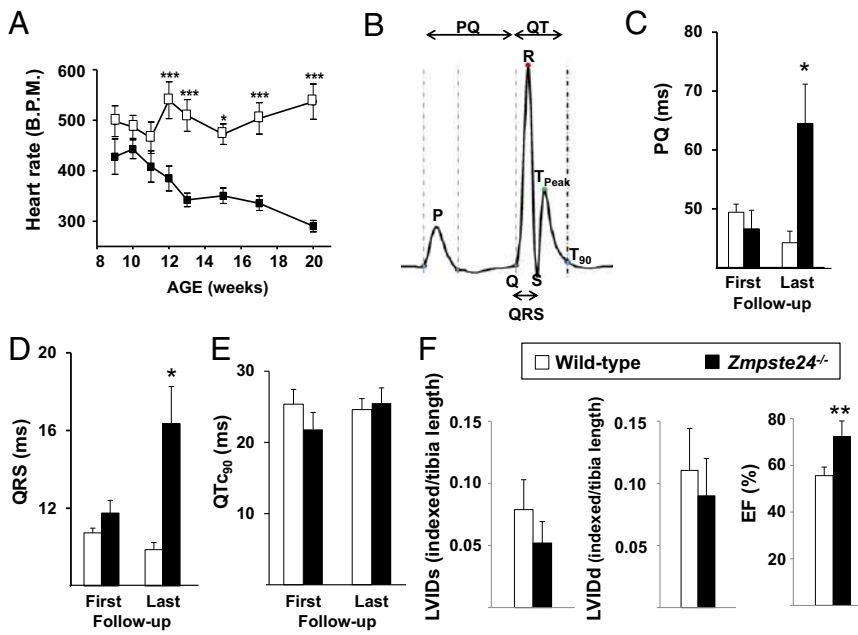


Fig. 3. *Zmpste24^{-/-}* mice show preserved cardiac function but develop severe bradycardia and cardiac conduction abnormalities. (A) Heart rate (bpm) in conscious mice. (B) Template ECG showing the intervals used to quantify (C) PQ, (D) QRS, and (E) heart rate-corrected QT at 90% of repolarization from T_{peak} ($QT_{\text{c}90}$) duration measured on the baseline ECG at the first follow-up (week 11; First) and the last follow-up (Last) (SI Appendix, SI Materials and Methods). (F) LVIDs, LVIDd, and EF determined by transthoracic echocardiography in 18- to 20-wk-old mice. * $P < 0.05$; ** $P < 0.01$; *** $P < 0.001$.

During both isoproterenol challenge (SI Appendix, Fig. S4) and recovery (SI Appendix, Fig. S5), *Zmpste24^{-/-}* mice showed increased prolongation of PQ and QRS intervals. Progeroid *Zmpste24^{-/-}* mice also developed age-dependent bradycardia in the absence of isoproterenol (Fig. 3A). In addition, at 18–20 wk of age, *Zmpste24^{-/-}* mice showed significant signs of defective cardiac conduction compared with age-matched controls manifested as prolonged PQ interval and QRS complex, without alterations to the QTc interval (Fig. 3 B–E and SI Appendix, Table S3).

Preserved Cardiac Function in *Zmpste24^{-/-}* Mice. Transthoracic echocardiography revealed no abnormalities in left ventricle end diastolic [left ventricular internal diameter at diastole (LVIDd)] or left ventricle end systolic [left ventricular internal diameter at systole (LVIDs)] parameters in progeroid *Zmpste24^{-/-}* mice (Fig. 3F). Likewise, *Zmpste24^{-/-}* mice had normal left ventricle mass, posterior wall and interventricular septal thickness at diastole (SI Appendix, Fig. S6A), and diastolic function but had a slightly higher left ventricle ejection fraction (EF) and fractional shortening than controls (Fig. 3F and SI Appendix, Fig. S6A), although within the normal range. The higher EF in progeroid mice might be explained by bradycardia, because longer diastolic intervals may favor such an increase. In fact, together, bradycardia and smaller body surface area in *Zmpste24^{-/-}* mice explain the significantly lower cardiac output compared with WT controls (SI Appendix, Fig. S6B). However, cardiac index, which relates the cardiac output of the left ventricle per minute to body surface area, was not different between progeroid and WT mice (SI Appendix, Fig. S6B). Time course studies showed no between-genotype differences in systolic or diastolic blood pressure (SI Appendix, Fig. S6C).

Ex Vivo Cellular Electrophysiology. We next conducted electrophysiology studies in cardiac multicellular preparations from *Zmpste24^{-/-}* mice to identify potential mechanisms underlying the arrhythmia risk associated with abnormal repolarization. No significant between-genotype differences were found in resting membrane potential, action potential (AP) amplitude, maximum velocity of depolarization (V_{max}), or AP duration in right or left ventricular samples (SI Appendix, Table S4). Moreover, APs recorded in right and left ventricular preparations were indistinguishable between genotypes (Fig. 4A). Interestingly, most *Zmpste24^{-/-}* ventricular preparations exhibited slow spontaneous automatic activity

at ~3 Hz (Fig. 4B). Also, *Zmpste24^{-/-}* left ventricle preparations displayed afterdepolarizations that led to triggered APs, contrasting with normal AP in controls (Fig. 4B and C).

We next analyzed transcription of genes encoding ion channel proteins involved in the different phases of the AP. Real-time quantitative PCR (qPCR) analysis in *Zmpste24^{-/-}* hearts revealed no significant between-group differences in mRNA expression of *Scn5A* (encoding the cardiac sodium channel $\text{Na}_V1.5$; involved in cell depolarization) or *KcnA5*, *KcnJ2*, *KcnD3*, and *KcnQ1* (encoding the potassium channels $K_v1.5$, $\text{Kir}2.1$, $\text{Kv}4.3$, and $\text{Kv}7.1$, respectively; all involved in AP repolarization); in contrast, *Zmpste24^{-/-}* hearts showed significant up-regulation of *KcnH2* (encoding the potassium channel $\text{Kv}11.1$, also known as human ether-à-go-go related gene (hERG; involved in AP repolarization) (SI Appendix, Fig. S7).

***Zmpste24^{-/-}* Mice Show Defective Sarcoplasmic Reticulum Ca^{2+} Handling.** We next investigated the role of intracellular Ca^{2+} handling in the observed *in vivo* afterdepolarizations and triggered APs in multicellular left ventricle *Zmpste24^{-/-}* preparations. Unlike WT cardiomyocytes, *Zmpste24^{-/-}* cardiomyocytes were unable to maintain stable Ca^{2+} transients at higher stimulation frequencies, an effect that was more prominent at 5 mM extracellular Ca^{2+} (Fig. 5A). To test whether this defect in *Zmpste24^{-/-}* cardiomyocytes was caused by unstable calcium release from the sarcoplasmic reticulum (SR) through the ryanodine receptor type 2 (RyR2) channel, we measured the frequency of spontaneous calcium waves at rest. However, we found no differences in the calcium wave frequency at any of the calcium concentrations examined (Fig. 5B). In line with these results, *Zmpste24* deficiency did not affect the transcript level of RyR2 (Fig. 5C), which is responsible for calcium release from the SR (12).

These findings suggested possible impairment of L-type Ca^{2+} currents (I_{Ca}) or Ca^{2+} uptake by the SR in *Zmpste24^{-/-}* cardiomyocytes as alternative causes for unstable calcium transients. Compared with WT controls, *Zmpste24^{-/-}* hearts expressed significantly lower transcript and protein levels of SR Ca^{2+} ATPase, whereas there was no alteration in transcript levels of *STIM1* (stromal interaction molecule component of the store-operated Ca^{2+} entry 1) and *Orai1* (component of the store-operated Ca^{2+} entry), essential regulators of Ca^{2+} release-activated Ca^{2+} channels (Fig. 5 C and D). We also analyzed the expression of

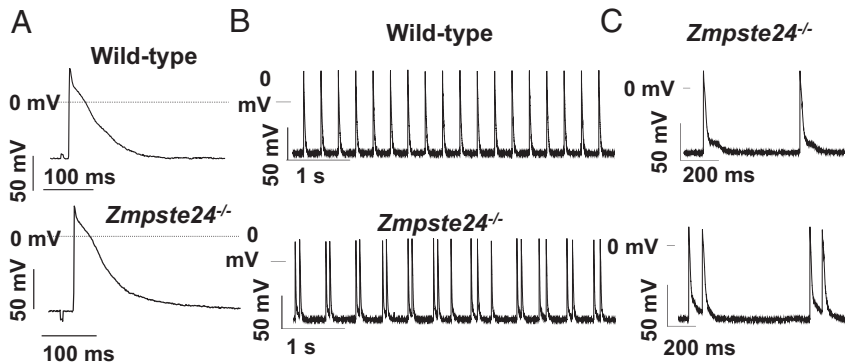


Fig. 4. Transmembrane APs recorded in multicellular left ventricular preparations. (A) Representative APs (3 Hz) from WT and *Zmpste24*^{-/-} mice. (B) Left ventricular preparations from *Zmpste24*^{-/-} mice displayed afterdepolarizations that occasionally yielded triggered APs (C, Lower).

calsequestrin 1 (*CSQ1*) and *CSQ2*, calcium-binding proteins of the SR that help this organelle store a very high amount of Ca^{2+} during relaxation in each contraction–relaxation cycle. Although *CSQ1* and *CSQ2* transcript levels were significantly lower in

Zmpste24^{-/-} hearts (Fig. 5C), no between-genotype differences were observed at the protein level (Fig. 5D). Likewise, peak I_{Ca} did not differ significantly between cardiomyocytes of the two genotypes (SI Appendix, Fig. S8).

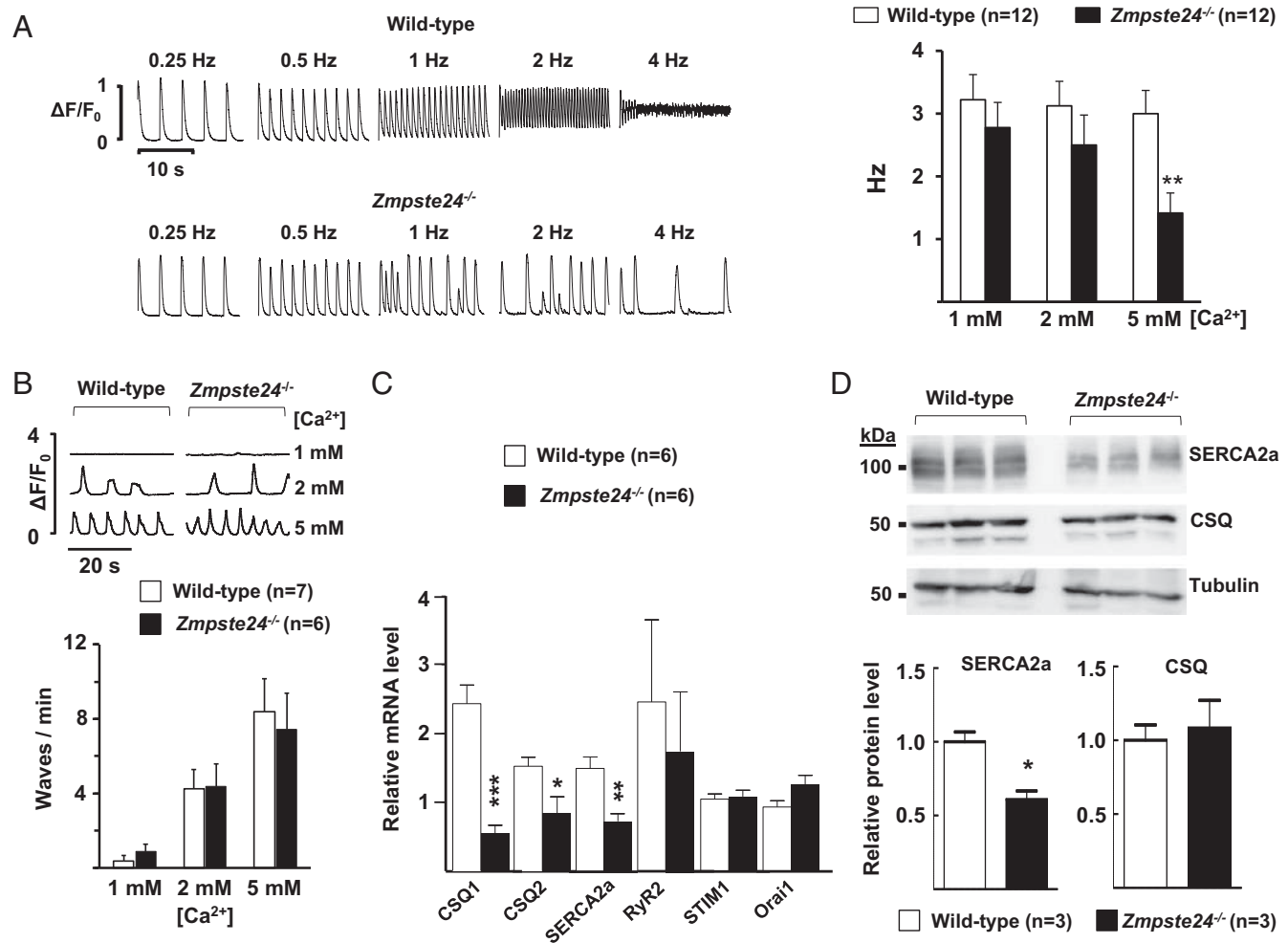


Fig. 5. Defective Ca^{2+} transients in *Zmpste24*^{-/-} cardiomyocytes. (A, Left) Analysis of beat to beat response stability in isolated mouse ventricular myocytes subjected to increasing stimulation frequencies. Representative examples of calcium transients recorded in the presence of 5 mM extracellular Ca^{2+} are shown. Irregular beat to beat responses start at lower frequencies in *Zmpste24*^{-/-} cardiomyocytes. (A, Right) The graph shows threshold frequencies (in hertz) for the induction of nonuniform beat to beat responses at the indicated Ca^{2+} concentrations. Responses were recorded in myocytes isolated from WT and *Zmpste24*^{-/-} mice (12 cells from six mice of each genotype). (B, Upper) Typical recordings of spontaneous calcium waves at the indicated Ca^{2+} concentrations. (B, Lower) Calcium dependency of the calcium wave frequency. Values are from seven WT mice ($n = 15$ cells) and six *Zmpste24*^{-/-} mice ($n = 14$ cells). (C) qPCR of heart tissue. (D) Western blot analysis of heart tissue. Representative blots are shown, and relative band intensity was quantified as described in SI Appendix, SI Materials and Methods. * $P < 0.05$; ** $P < 0.01$; *** $P < 0.001$.

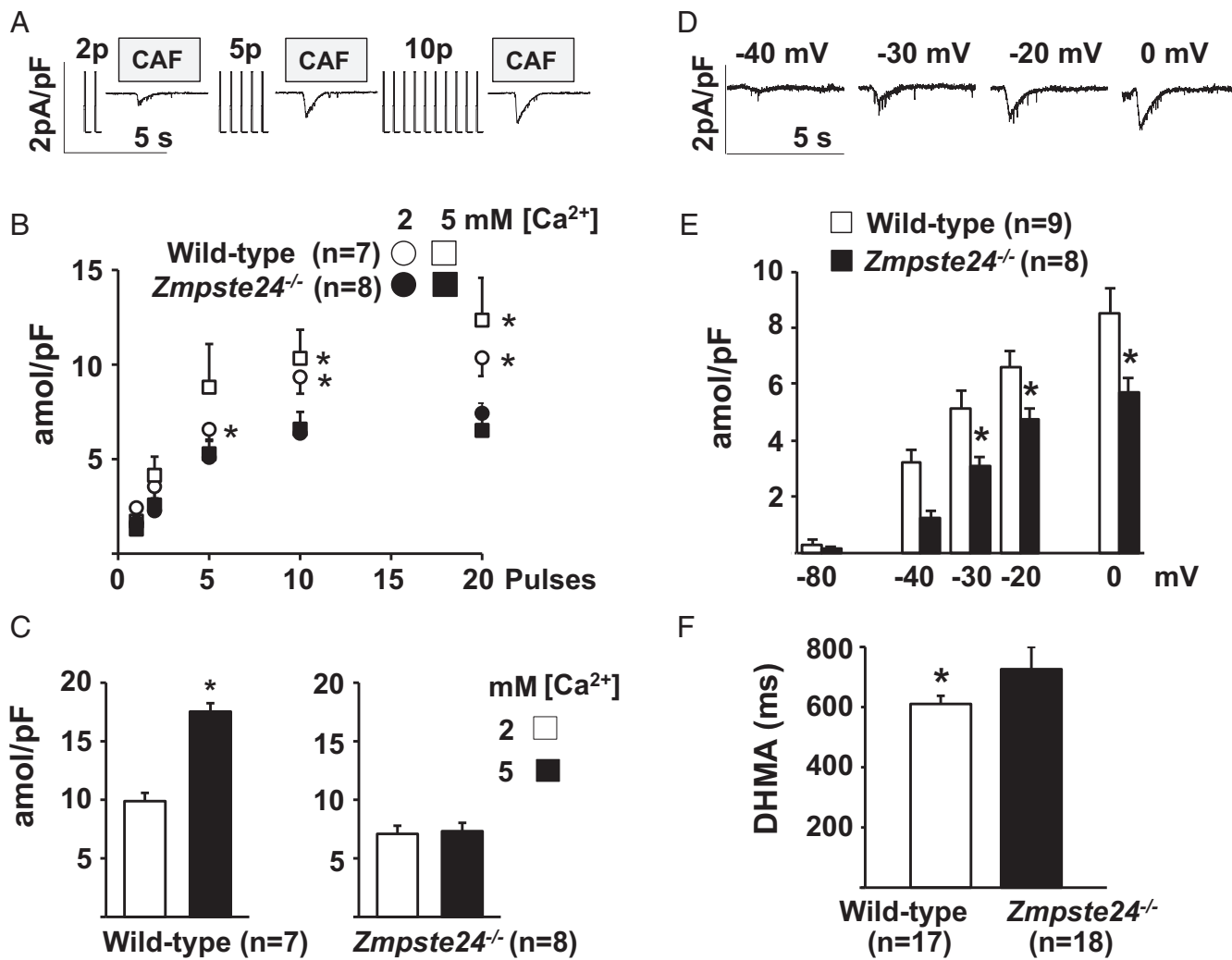


Fig. 6. Reduced maximal SR Ca^{2+} uptake in $Zmpste24^{-/-}$ cardiomyocytes. SR calcium loading capacity in isolated ventricular myocytes. (A–C) Calcium loading measured as a function of the number of stimulation pulses used for SR loading. (A) Representative caffeine (CAF)-induced currents recorded after SR reloading with the indicated number of stimulation pulses. Transient exposure to CAF was used to release SR calcium content before reloading and measure loading after the train of stimulation pulses. (B) Time integral of CAF-induced currents recorded after SR reloading with the indicated stimulation pulses. Data were obtained from seven $Zmpste24^{-/-}$ and eight WT myocytes (from $n = 5$ mice) exposed consecutively to 2 and 5 mM extracellular Ca^{2+} . Time integrals were converted to amoles and normalized to cellular capacitance (in picofarads). (C) Effect of extracellular calcium concentration on the time integral of CAF-induced current at steady state (after ≥ 30 stimulation pulses). (D–F) Calcium loading measured as a function of membrane potential. (D) Representative CAF-induced currents recorded after SR loading with a 5-s depolarization to the indicated membrane potentials. (E) Time integral of CAF-induced current recorded in the presence of 2 mM extracellular Ca^{2+} after SR reloading at rest (-80 mV) and after depolarizing to the indicated voltage. Data were obtained from eight $Zmpste24^{-/-}$ myocytes ($n = 5$ mice) and nine WT myocytes ($n = 6$ mice). (F) Mean calcium transient duration at half-maximal amplitude (DHMA) recorded in myocytes paced at 0.5 Hz (17 WT and 18 $Zmpste24^{-/-}$ myocytes from $n = 6$ mice per group). * $P < 0.05$.

To determine SR Ca^{2+} reloading function in ventricular cardiomyocytes, we loaded the SR by exposing cells to an increasing number of stimulation pulses and estimated the resulting Ca^{2+} load from caffeine-elicited inward current traces (Fig. 6A). SR reloading function was significantly weaker in $Zmpste24^{-/-}$ cardiomyocytes than in WT cells after 5, 10, and 20 stimulation pulses (Fig. 6B), and the defective response was still more apparent after ≥ 30 stimulation pulses (Fig. 6C). Significantly lower SR Ca^{2+} loading in $Zmpste24^{-/-}$ cardiomyocytes was also evident from caffeine-elicited current traces recorded after loading the SR by depolarizing the membrane potential for 5 s to -40 , -30 , -20 , or 0 mV (Fig. 6D and E). In addition, intracellular Ca^{2+} transients recorded in isolated cardiomyocytes paced at 0.5 Hz revealed a significantly longer Ca^{2+} -transient duration (at half-maximal amplitude) in $Zmpste24^{-/-}$ cells (Fig. 6F).

Finally, we measured the SR Ca^{2+} release-dependent inactivation of the I_{Ca} in response to consecutive stimulation pulses given after clearance of SR Ca^{2+} (Fig. 7A) to assess the feedback of SR calcium release on I_{Ca} inactivation. As expected, current traces recorded in WT cardiomyocytes showed a faster rate of I_{Ca} inactivation as the number of pulses used for SR reload increased from 1 (p1) to 30 (p30) (Fig. 7B). In contrast, the effect of SR loading on the I_{Ca} inactivation rate in $Zmpste24^{-/-}$ cardiomyocytes was very modest (Fig. 7B). Accordingly, the time constant for I_{Ca} inactivation decreased progressively with increasing pulse number in WT but not $Zmpste24^{-/-}$ cardiomyocytes (Fig. 7C). Moreover, the amplitude of the intracellular Ca^{2+} transient induced by repeated stimulation at 0.5 Hz was significantly lower in $Zmpste24^{-/-}$ cardiomyocytes (Fig. 7D). Together, these findings indicate that SR Ca^{2+} uptake and release are blunted in $Zmpste24^{-/-}$ cardiomyocytes, which also explains the failure of acute isoproterenol

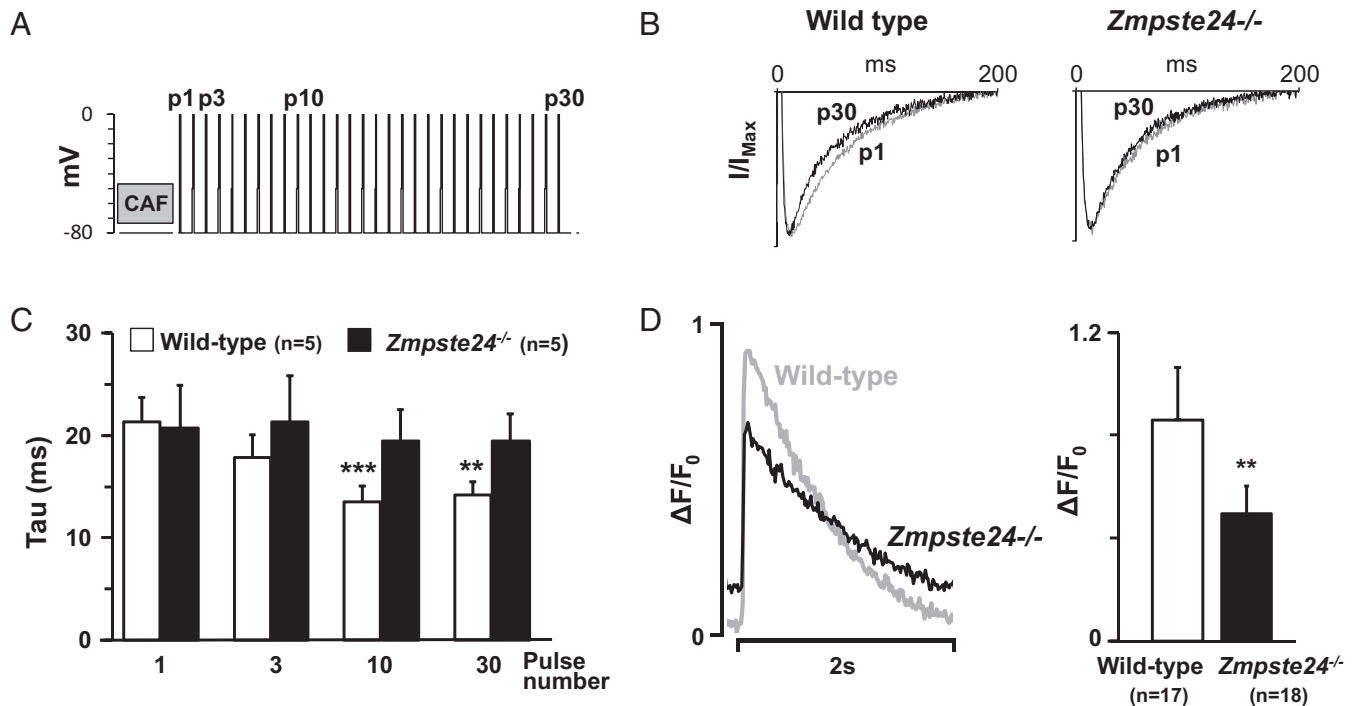


Fig. 7. Impaired SR calcium release-dependent inactivation of I_{Ca} in isolated $Zmpste24^{-/-}$ myocytes. (A) Protocol to measure the effect of SR calcium loading on I_{Ca} inactivation. SR calcium content was released with caffeine (CAF) and reloaded with a train of stimulation pulses. (B) Representative superimposed I_{Ca} recordings on p1 and p30. Currents were normalized to their peak values and fitted to a double-exponential equation. (C) Dependency of time constant (τ) for fast I_{Ca} inactivation on indicated pulses. (D) Representative calcium transient ($\Delta F/F_0$) recordings from myocytes paced at 0.5 Hz (Left) and calcium transient amplitude quantification (Right). Indicated cardiomyocytes are from $n = 6$ mice per genotype. ** $P < 0.01$; *** $P < 0.001$.

treatment to induce ventricular arrhythmia, despite abnormal repolarization.

Abnormal Connexin43 Localization in the Hearts of $Zmpste24^{-/-}$ Mice and HGPS Patients. To further investigate conduction alterations in progeria, we performed immunohistopathological studies in heart tissue. Cardiomyocyte size was estimated by quantifying their cross-sectional area in heart sections as well as the membrane capacitance, which is linearly proportional to the plasma membrane area and cell size. Because $Zmpste24^{-/-}$ mice are smaller than age-matched controls (9, 11), we normalized results by tibia length. Normalized cross-sectional area and membrane capacitance were similar in cardiomyocytes of both genotypes (SI Appendix, Fig. S9). We also performed Mallory's trichrome staining, which revealed normal chambers, ventricular walls, and myocardial fiber arrangement in $Zmpste24^{-/-}$ hearts (SI Appendix, Fig. S10 A and B). Moreover, Mallory's trichrome staining did not reveal increased fibrosis in the ventricular interstitium (SI Appendix, Fig. S10B) or key structures involved in cardiac conduction, such as the atrioventricular node and the main His bundles (SI Appendix, Fig. S10C), which might have explained conduction abnormalities in $Zmpste24^{-/-}$ mice. However, consistent with previous studies in HGPS patients (13), $Zmpste24^{-/-}$ mice showed extensive fibrosis in the tunica media of the major coronary arteries (SI Appendix, Fig. S11A) and discontinuous and weak expression of smooth muscle actin within the medial arterial layer (SI Appendix, Fig. S11B).

Another possible explanation for the observed cardiac conduction anomalies is altered expression of intercalated disk proteins that play a key role in intercellular connectivity, such as the gap junction protein connexin43 (Cx43) and plakoglobin, as well as cytoskeletal desmosome-interacting proteins, such as desmin, a class III intermediate filament connected to A-type lamins through Nesprin/Sun protein complexes. Western blot

analysis in progeroid hearts revealed a significant approximately twofold increase in Cx43 expression without changes in plakoglobin or desmin (SI Appendix, Fig. S12). Remarkably, compared with WT controls, $Zmpste24^{-/-}$ cardiomyocytes exhibited marked mislocalization of Cx43 to the cytoplasm and the lateral long axis as revealed by double immunofluorescence to simultaneously detect Cx43 and N-Cadherin (Fig. 8A). Quantification of digital images revealed less Cx43/N-Cadherin colocalization in the hearts of progeroid mice than in WT controls (Fig. 8E).

Profound Cx43 mislocalization was also revealed by immunostaining of left ventricle specimens obtained from two HGPS patients at autopsy. In these patients, Cx43 was abundantly associated with the perinuclear rim (Fig. 8 B–D), which is its trafficking origin for subsequent targeting to the intercalated disks (14) (Discussion). Quantification of digital images confirmed a low percentage of Cx43/N-Cadherin colocalization in HGPS hearts (Fig. 8E). Defective cardiomyocyte connectivity associated to Cx43 mislocalization may contribute to cardiac conduction defects in progeria (Discussion).

Discussion

HGPS is a devastating genetic disease resulting from abnormal processing of prelamin A, which is characterized by premature cardiovascular disease and death at an average age of 14.6 y old (4). Here, we provide a comprehensive analysis of electrocardiographic abnormalities and underlying molecular changes at different stages of HGPS. Our findings may have implications for the risk of premature death in HGPS patients and potentially, normal aging, because defective prelamin A processing has also been revealed in cells and tissues of normally aging non-HGPS individuals (reviewed in refs. 2 and 7). A previous study identified repolarization abnormalities in 3 of 15 HGPS patients with the “classical” *LMNA* c.1824C > T mutation (3). Here, we confirm and extend these findings through a rigorous examination of a new

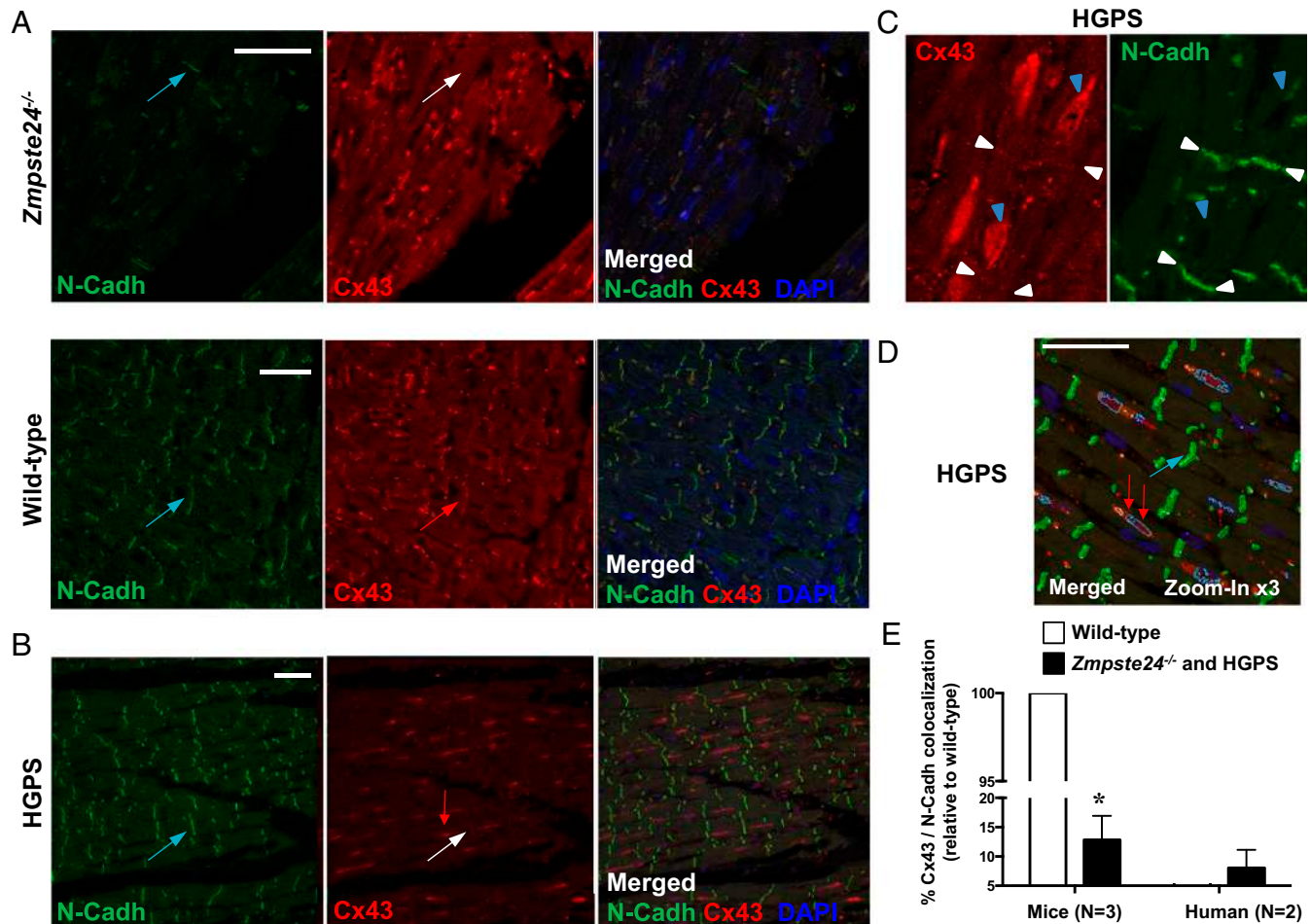


Fig. 8. Abnormal localization of Cx43 in hearts of progeroid *Zmpste24^{-/-}* mice and HGPS patients. (*A* and *B*) Double immunofluorescence of left ventricle sections from mice of the indicated genotype and HGPS patients to detect N-Cadherin (N-Cadh; green in *Left*) and Cx43 (red in *Center*). *Right* shows merged images, with DAPI staining of nuclei (blue). (*A*) Cx43 lateralization was evident in *Zmpste24^{-/-}* mice. Blue arrows mark examples of intercalated disk areas (N-Cadh positive). The white arrow in the *Zmpste24^{-/-}* image marks an intercalated disk without Cx43 expression, and the red arrow in the WT image marks an intercalated disk with abundant Cx43 expression. (*B*) Representative images illustrating loss of Cx43/N-Cadh colocalization in HGPS heart. Blue arrow and white arrow are as in *A*. The red arrow marks a Cx43-positive area, which does not colocalize with N-Cadh. (*C*) Magnified view of an HGPS heart section. Blue arrowheads mark examples of predominant Cx43 expression near nuclei. White arrowheads mark examples of scant Cx43/N-Cadh colocalization at intercalated disks. (*D*) Automatic image segmentation of an HGPS heart section used for quantification of Cx43/N-Cadh colocalization. Green, red, and dark blue blob boundaries correspond to positive staining for N-Cadh, Cx43, and nuclei, respectively. Cyan blob boundaries represent areas showing Cx43/nuclei colocalization. (Scale bars: 50 μ m.) (*E*) Percentage of Cx43/N-Cadh colocalization at the intercalated disks estimated by quantifying automatically segmented images. Results are represented relative to WT (>100); *n* = 3 WT and *Zmpste24^{-/-}* mice and *n* = 2 HGPS patients were analyzed (*n* = 5 sections per individual). **P* < 0.001.

cohort of 15 HGPS patients carrying the same mutation. One-half of the patients showed overt repolarization abnormalities in at least one ECG compatible with coronary artery disease (ST depression/elevation and negative and biphasic T waves). Repolarization abnormalities in HGPS patients were strongly evident at advanced disease stages. We also detected prominent mislocalization of Cx43 in left ventricle specimens obtained at autopsy from diseased HGPS patients; Cx43 mislocalization was also observed in the hearts of progeroid *Zmpste24^{-/-}* mice and is indicative of defective cardiac conduction in progeria (see below).

Animal models resembling the clinical phenotype of HGPS patients are central to understanding the underlying mechanisms of the disease and developing novel therapies. Our analysis of the well-established *Zmpste24^{-/-}* mouse model of progeria caused by prelamin A accumulation (9, 11) revealed the progressive development of cardiac rhythm alterations that can lead to premature death. *Zmpste24^{-/-}* hearts and cardiomyocytes showed the following specific alterations: (*i*) T-wave repolarization abnormalities, which were also present in one-half of HGPS pa-

tients; (*ii*) prolonged PQ interval and wide QRS complex; (*iii*) development of bradycardia-related premature ventricular complexes and slow-rate polymorphic ventricular rhythms at late disease stages in the absence of ventricular arrhythmias during isoproterenol challenge; (*iv*) automatic spontaneous ventricular activity and afterdepolarizations ex vivo, which were associated with significantly slowed I_{Ca} inactivation and reduced amplitude of the intracellular Ca²⁺ transient; and (*v*) mislocalization of Cx43 in the heart.

Notably, some characteristics of the progeroid *Zmpste24^{-/-}* mouse heart are also present in HGPS patients and frequently observed in normal aging; these characteristics include extensive fibrosis and loss of smooth muscle cells in coronary arteries, defective calcium homeostasis, progressive development of repolarization defects, and Cx43 mislocalization (15–17). Overt repolarization abnormalities in ST T waves and T-wave flattening in mice did not increase the risk of isoproterenol-triggered ventricular arrhythmia. However, T-wave alterations are well-known to increase the risk of lethal ventricular arrhythmias

during ischemia (18), which might contribute to premature death in HGPS patients from myocardial infarction, one of the main causes of death in this population. T-wave abnormalities might be explained at least in part by an altered repolarization pattern brought about by two opposing ion channel changes observed in the hearts of *Zmpste24*^{-/-} mice: on the one hand, the significant up-regulation of *Kcnh2*, which encodes the hERG channel responsible for I_{Kr} , would help terminate the AP plateau and shorten repolarization (19), and on the other hand, the observed slow I_{Ca} inactivation would tend to prolong the plateau and delay repolarization (20). Importantly, an abnormally long QTc interval was observed in only 1 of 51 ECGs from 15 HGPS patients and occurred in the context of ischemia and significant repolarization anomalies. Consistently, we observed no significant QTc prolongation in *Zmpste24*^{-/-} mice, in agreement with the normal AP duration observed in *Zmpste24*^{-/-} ventricular cardiomyocytes and the majority of ECG traces from HGPS patients. Although we documented significant QRS complex widening in progeroid mice, it is important to note that the high-amplitude QRS complex in the mouse ECG represents not only the spread of depolarization across the ventricle but also, the early phase of repolarization (21). We, therefore, carefully examined QRS complex and QT duration (QT₉₀) (Fig. 3 B–E) to detect any significant increases in both parameters. However, mouse and human QT intervals must be compared with caution.

The occurrence of bradycardia-related premature ventricular complexes in *Zmpste24*^{-/-} mice during recovery after isoproterenol shows a significant suppression of normal pacemaker activity, with emergence of ventricular ectopic escape discharges. Isoproterenol-induced heart rate increase *in vivo* is associated with increases in intracellular Na⁺ and Ca²⁺ concentration (22); these changes, in the presence of the postisoproterenol-induced bradycardia, likely contributed to the escape discharges and premature ventricular complexes arising from the Purkinje system (*SI Appendix*, Fig. S3). Our ex vivo experiments with multicellular ventricular preparations showed afterdepolarizations during spontaneous ventricular activity at ~3 Hz, which is similar to the cycle length after isoproterenol treatment *in vivo*. Although we were unable to establish the exact origin of these ventricular afterdepolarizations, the *in vivo* data support involvement of the Purkinje system, consistent with slow idioventricular discharges (cycle length = 266.38) (*SI Appendix*, Fig. S3) arising from varying Purkinje locations.

Connexins are the pore-forming subunits of gap junctions and essential for proper intercellular electrical coupling between cardiomyocytes and AP spread during each cardiac cycle (23, 24). Cx43 is the major connexin expressed in the ventricles. Its abnormal expression, typically involving down-regulation and heterogeneous redistribution to the lateral cardiomyocyte membrane, is associated with different forms of chronic heart disease (hypertrophic, dilated, and ischemic cardiomyopathy) and even aging (24–26). Defective Cx43 expression results in electrical defects in the myocardium and contributes to arrhythmogenesis. Therefore, Cx43 mislocalization in the heart may explain, at least partly, the prolongation of PQ interval and QRS complex in *Zmpste24*^{-/-} mice. Interestingly, reduced gap junction coupling accompanied by Cx43 lateralization has been linked to reduced functional expression of the alpha subunit (Nav1.5) of the cardiac sodium channel at the intercalated disk (27), and the reduced sodium current is likely to have contributed to the significantly impaired atrioventricular and intraventricular conduction in *Zmpste24*^{-/-} mice. Previous computer simulations (28) suggest that, even in the presence of Cx43 mislocalization and low Nav1.5 expression, a normal peak I_{Ca} with slow inactivation and reduced Ca²⁺ transients could maintain relatively safe conduction in the ventricles of *Zmpste24*^{-/-} mice, albeit at a reduced velocity. However, a high intracellular Ca²⁺ concentration would have compromised propagation safety and caused earlier block as ob-

served for reduced intercellular coupling (28). Because the intercalated disk is regarded as a functional unit, with gap junction formation requiring the presence of neighboring mechanical junctions (29), we tested the expression of desmin and plakophilin-2. However, our Western blot analysis in *Zmpste24*^{-/-} hearts revealed no alterations in the expression of these proteins.

Consistent with the findings in *Zmpste24*^{-/-} mice, immunofluorescence studies in left ventricle specimens from deceased HGPS patients revealed abnormal cellular distribution of Cx43 to a predominantly perinuclear localization. Because Cx43 is packaged into vesicles at the perinuclear trans-Golgi network and then transported to the intercalated disk (14), our findings suggest that abnormal prelamin A processing causes defective Cx43 targeting to its distinctive microdomain at the gap junctions. Additional *LMNA* mutations might also cause cardiomyopathy by altering connexin expression and/or cellular localization. For example, transgenic mice expressing the lamin A N195K mutant, which causes dilated cardiomyopathy with conduction system disease in humans, die at an early age because of arrhythmia, and such a phenotype correlates with cardiac Cx43 and Cx40 misexpression and/or mislocalization (30). Future studies are warranted to elucidate the mechanism causing defective Cx43 microdomain targeting to gap junctions and their contribution to abnormal cardiac conduction in progeria.

Some of the nuclear envelope alterations in the heart associated with prelamin A or progerin expression also occur during normal aging (15–17), suggesting that shared mechanisms might cause cardiac alterations in HGPS patients and the geriatric population. Consistent with this idea, prelamin A and progerin are both produced in the cells of normally aging individuals, thus raising the possibility that altered lamin A processing contributes to normal aging and associated cardiovascular disease (reviewed in refs. 2 and 7). Much like in normal human aging, progeroid *Zmpste24*^{-/-} mice develop coronary fibrosis, bradycardia, and severe conduction abnormalities. Cardiac conduction abnormalities also arise during aging in WT mice and are associated with an increased incidence of arrhythmias (31). However, Ca²⁺ transients differ between *Zmpste24*^{-/-} mice and normally aging WT mice (32), with *Zmpste24*^{-/-} cardiomyocytes being unable to maintain stable Ca²⁺ transients at 4 Hz. Ventricular cardiomyocytes from aged WT mice also have a significantly higher incidence of spontaneous Ca²⁺ sparks than cells from young animals; however, we did not observe a similar difference between progeroid mice and age-matched controls. *Zmpste24*^{-/-} mice show weakened I_{Ca} inactivation and defective SR Ca²⁺ uptake and release, features also observed in aging human atrial myocytes (15). In line with these findings, Ca²⁺ transient amplitudes are reduced in progeroid mice (Fig. 6), aged WT mice (32), and aged human atrial cardiomyocytes (15).

The progressively developing bradycardia and deteriorating cardiac conduction in progeroid mice also resemble clinical rhythm abnormalities observed in the elderly (16, 17). Although the most common age-related cardiac conduction abnormality in humans is degenerative fibrosis (33), *Zmpste24*^{-/-} mice did not show abnormal fibrosis in the ventricular interstitium or the major conduction structures. However, in line with observations in HGPS patients (13), the coronary arteries of *Zmpste24*^{-/-} mice showed extensive fibrosis and reduced accumulation of smooth muscle cells, potential causes of vascular stiffening, reduced coronary flow, and abnormal impulse generation in the sinoatrial node and conduction in the atria and ventricles. The latter may have also contributed to T-wave alterations, especially during isoproterenol challenge, as well as progressive development of bradycardia in progeroid *Zmpste24*^{-/-} mice. In fact, human patients with coronary artery disease show a high prevalence of conduction abnormalities, such as atrioventricular or sinoatrial block (34).

We provide a comprehensive characterization of cardiac abnormalities in HGPS patients and progeroid *Zmpste24^{-/-}* mice, identifying a number of cellular and molecular alterations in both species that are likely to contribute to defective cardiac repolarization and conduction in progeria. Future studies are warranted to establish direct causal connections between the presence of unprocessed prelamin A or progerin and the cardiac abnormalities associated with HGPS, with the goal of identifying novel targets for therapeutic intervention. Based on our findings, major efforts should be placed into elucidating the mechanisms causing Cx43 mislocalization in the heart of progeroid mice and HGPS patients. These studies may pave the way to developing efficient therapies to improve cardiac conduction in progeria.

Although ion channels are highly conserved between humans and mice, significant electrophysiological differences exist (35), making it difficult to translate mouse findings to the clinical arena. For example, although we observed a tendency toward a slower heart rate in older HGPS patients with longer follow-up, HGPS patients did not show the bradycardia and other conduction abnormalities that appeared progressively in *Zmpste24^{-/-}* mice. This difference might be due to the lack of sequential ECG assessment in humans until very advanced disease stages. Indeed, human left ventricle specimens obtained by autopsy revealed reduced localization of Cx43 at gap junctions, consistent with altered ventricular conduction velocity.

Continuous telemetry and other invasive electrophysiological measurements would have been desirable in *Zmpste24^{-/-}* mice. However, these animals show severe body weight loss (body weight of ~9 g at late stages compared with ~30 g in age-matched WT controls) and are physically extremely fragile, precluding the use of commercially available telemetry systems or any other invasive approaches to register specific arrhythmias forecasting premature death. The physical deterioration of HGPS patients also limits

implementation of any invasive measurements (e.g., implantable loop recordings) to further study rhythm abnormalities.

Materials and Methods

Clinical information from children with HGPS was obtained from The Progeria Research Foundation Medical and Research Database (principal investigator L.B.G.) and approved by the Rhode Island Hospital and Brown University Institutional Review Boards (Providence, RI). All participants or parents provided written informed consent in the primary language of the participant or parent. When appropriate, interpreters were used for consenting. At least one ECG recorded no more than 3 y before death was obtained from each of 15 HGPS patients. Thirteen gender- and age-matched control volunteers were weighed, and ECG traces were recorded for comparison. All control volunteers or parents provided written informed consent. Animal studies were carried out in male *Zmpste24^{-/-}* mice (11) and age-matched WT male littermates (all C57BL/6). Mice were reared and housed in accordance with institutional guidelines and regulations and all procedures with mice were approved by the Centro Nacional de Investigaciones Cardiovasculares Carlos III (CNIC) Ethical Committee. All other detailed materials and methods are described in *SI Appendix, SI Materials and Methods*.

ACKNOWLEDGMENTS. We thank María Jesús Andrés for technical assistance and help with art work, Susan Campbell for assistance with patient information, Maite Dubraska for assistance with blood sampling and ECG in control subjects, Inés Ortega and Virginia Zorita for animal maintenance and care, and Simon Bartlett for English editing. This work was supported by Spanish Ministry of Economy and Competitiveness (MINECO) Grants SAF2010-16044 and SAF2013-46663-R (to V.A.), SAF2011-30312 and SAF2014-58286-C2-1-R (to L.H.-M.), SAF2011-30088 (to E.D.), and SAF2014-52413-R (to C.L.-O.) and Fondo de Investigación Sanitaria del Instituto de Salud Carlos III Grants RD12/0042/0028 (to V.A.), RD12/0042/0011 (to J.T.), and RD12/0042/0002 (to L.H.-M.), with cofunding from the Fondo Europeo de Desarrollo Regional and the Progeria Research Foundation. J.A.G. is the recipient of a U-Mobility Grant from the Marie Curie cofunding of Regional, National and International Programme (Grant 246550). The Instituto Universitario de Oncología is supported by Obra Social Cajastur. The CNIC is supported by the MINECO and the Pro CNIC Foundation, and it is a Severo Ochoa Center of Excellence (MINECO Award SEV-2015-0505).

1. Andrés V, González JM (2009) Role of A-type lamins in signaling, transcription, and chromatin organization. *J Cell Biol* 187(7):945–957.
2. Trigueros-Motos L, González JM, Rivera J, Andrés V (2011) Hutchinson-Gilford progeria syndrome, cardiovascular disease and oxidative stress. *Front Biosci (Schol Ed)* 3:1285–1297.
3. Merideth MA, et al. (2008) Phenotype and course of Hutchinson-Gilford progeria syndrome. *N Engl J Med* 358(6):592–604.
4. Gordon LB, et al.; Progeria Clinical Trials Collaborative (2014) Impact of farnesylation inhibitors on survival in Hutchinson-Gilford progeria syndrome. *Circulation* 130(1):27–34.
5. Barrowman J, Wiley PA, Hudon-Miller SE, Hrycyna CA, Michaelis S (2012) Human ZMPSTE24 disease mutations: Residual proteolytic activity correlates with disease severity. *Hum Mol Genet* 21(18):4084–4093.
6. Osorio FG, et al. (2011) Cell autonomous and systemic factors in progeria development. *Biochem Soc Trans* 39(6):1710–1714.
7. Gordon LB, Rothman FG, López-Otín C, Misteli T (2014) Progeria: A paradigm for translational medicine. *Cell* 156(3):400–407.
8. Zhang H, Kieckhaefer JE, Cao K (2013) Mouse models of laminopathies. *Aging Cell* 12(1):2–10.
9. Varela I, et al. (2005) Accelerated ageing in mice deficient in Zmpste24 protease is linked to p53 signalling activation. *Nature* 437(7058):564–568.
10. Villa-Bellosta R, et al. (2013) Defective extracellular pyrophosphate metabolism promotes vascular calcification in a mouse model of Hutchinson-Gilford progeria syndrome that is ameliorated on pyrophosphate treatment. *Circulation* 127(24):2442–2451.
11. Pendás AM, et al. (2002) Defective prelamin A processing and muscular and adipocyte alterations in Zmpste24 metalloproteinase-deficient mice. *Nat Genet* 31(1):94–99.
12. Willis BC, et al. (2016) Constitutive intracellular Na⁺ excess in purkinje cells promotes arrhythmogenesis at lower levels of stress than ventricular myocytes from mice with catecholaminergic polymorphic ventricular tachycardia. *Circulation* 133(24):2348–2359.
13. Olive M, et al. (2010) Cardiovascular pathology in Hutchinson-Gilford progeria: Correlation with the vascular pathology of aging. *Arterioscler Thromb Vasc Biol* 30(11):2301–2309.
14. Smyth JW, et al. (2012) Actin cytoskeleton rest stops regulate anterograde traffic of connexin 43 vesicles to the plasma membrane. *Circ Res* 110(7):978–989.
15. Herranz-Martínez A, et al. (2015) Ageing is associated with deterioration of calcium homeostasis in isolated human right atrial myocytes. *Cardiovasc Res* 106(1):76–86.
16. Jensen PN, et al. (2014) Incidence of and risk factors for sick sinus syndrome in the general population. *J Am Coll Cardiol* 64(6):531–538.
17. Strait JB, Lakatta EG (2012) Aging-associated cardiovascular changes and their relationship to heart failure. *Heart Fail Clin* 8(1):143–164.
18. Verrier RL, Ikeda T (2013) Ambulatory ECG-based T-wave alternans monitoring for risk assessment and guiding medical therapy: Mechanisms and clinical applications. *Prog Cardiovasc Dis* 56(2):172–185.
19. Perry M, Sanguinetti M, Mitcheson J (2010) Revealing the structural basis of action of hERG potassium channel activators and blockers. *J Physiol* 588(Pt 17):3157–3167.
20. Madhvani RV, et al. (2015) Targeting the late component of the cardiac L-type Ca²⁺ current to suppress early afterdepolarizations. *J Gen Physiol* 145(5):395–404.
21. Mitchell GF, Jeron A, Koren G (1998) Measurement of heart rate and Q-T interval in the conscious mouse. *Am J Physiol* 274(3 Pt 2):H747–H751.
22. Vassalle M (1977) The relationship among cardiac pacemakers. Overdrive suppression. *Circ Res* 41(3):269–277.
23. Vaideya D, et al. (2001) Null mutation of connexin43 causes slow propagation of ventricular activation in the late stages of mouse embryonic development. *Circ Res* 88(11):1196–1202.
24. Fontes MS, van Veen TA, de Bakker JM, van Rijen HV (2012) Functional consequences of abnormal Cx43 expression in the heart. *Biochim Biophys Acta* 1818(8):2020–2029.
25. Peters NS (1996) New insights into myocardial arrhythmogenesis: Distribution of gap-junctional coupling in normal, ischaemic and hypertrophied human hearts. *Clin Sci (Lond)* 90(6):447–452.
26. Saffitz JE, Schuessler RB, Yamada KA (1999) Mechanisms of remodeling of gap junction distributions and the development of anatomic substrates of arrhythmias. *Cardiovasc Res* 42(2):309–317.
27. Cerrone M, et al. (2012) Sodium current deficit and arrhythmogenesis in a murine model of plakophilin-2 haploinsufficiency. *Cardiovasc Res* 95(4):460–468.
28. Shaw RM, Rudy Y (1997) Ionic mechanisms of propagation in cardiac tissue. Roles of the sodium and L-type calcium currents during reduced excitability and decreased gap junction coupling. *Circ Res* 81(5):727–741.
29. Delmar M, McKenna WJ (2010) The cardiac desmosome and arrhythmogenic cardiomyopathies: From gene to disease. *Circ Res* 107(6):700–714.
30. Mounkes LC, Kozlov SV, Rottman JN, Stewart CL (2005) Expression of an LMNA-N195K variant of A-type lamins results in cardiac conduction defects and death in mice. *Hum Mol Genet* 14(15):2167–2180.
31. Signore S, et al. (2015) Late Na⁺ current and protracted electrical recovery are critical determinants of the aging myopathy. *Nat Commun* 6:8803.
32. Howlett SE, Grandy SA, Ferrier GR (2006) Calcium spark properties in ventricular myocytes are altered in aged mice. *Am J Physiol Heart Circ Physiol* 290(4):H1566–H1574.
33. Ferrer MI (1982) The etiology and natural history of sinus node disorders. *Arch Intern Med* 142(2):371–372.
34. Hsueh CW, Lee WL, Chen YT, Ting CT (2001) The incidence of coronary artery disease in patients with symptomatic bradyarrhythmias. *Jpn Heart J* 42(4):417–423.
35. London B (2001) Cardiac arrhythmias: From (transgenic) mice to men. *J Cardiovasc Electrophysiol* 12(9):1089–1091.